NANO LETTERS

2007
Vol. 7, No. 12
3891−3894

Variation of Radial Elasticity in Multiwalled Carbon Nanotubes

Lata Muthaswami,[†] Yuegui Zheng,[†] Robert Vajtai,[‡] G. Shehkawat,[†,||] Pulickel Ajayan,[§] and Robert E. Geer*[,†]

College of Nanoscale Science and Engineering, University at Albany, Albany, New York 12203, and Rensselaer Nanotechnology Center, Department of Materials Science and Engineering, Rensselaer Polytechnic Institute, Troy, New York 12180

Received August 10, 2007; Revised Manuscript Received October 31, 2007

ABSTRACT

Correlations between the local diameter and local radial elastic modulus in multiwalled carbon nanotubes (MWNTs) were investigated via ultrasonic force microscopy. Spatial cross-correlation analysis showed that local radial modulus variations were inversely correlated with local diameter gradients ("bamboo" structures) in MWNTs grown via chemical vapor deposition (CVD). In contrast, uniform MWNTs grown via arc discharge exhibited no such correlation, indicating that reductions of elastic modulus previously reported for CVD-grown MWNTs originated from increased defect density associated with local increases in diameter.

Since their discovery[1] carbon single-walled nanotubes (SWNTs) and multiwalled nanotubes (MWNTs) have attracted enormous scientific interest due to their unique mechanical, electrical, and thermal properties. Theoretical and experimental investigations estimate the (axial) Young's modulus of ideal SWNTs and MWNTs to be in the 1 TPa range.[2−5] However, MWNTs grown via chemical vapor deposition (CVD) that exhibited local variations of the nanotube diameter (termed "bamboo" structures) possessed an average bending modulus an order of magnitude smaller than comparable MWNTs that exhibited a uniform radial microstructure deposited via an arc-discharge (AD) method.[6] This has been attributed the reduction in modulus for CVD-grown MWNTs to high-crystalline defect densities associated with local changes in diameter. However, the experimental approach employed in that study was not able to spatially resolve variation of modulus within a single MWNT. Modulus measurements based on atomic force microscopy (AFM), although experimentally challenging, have inherently high-spatial resolution. Several groups have pioneered this approach to image variations of mechanical response inside an individual nanotube.[7−9] However, no studies have been reported that statistically correlate nanoscale variations in elastic modulus with local variations in radial microstructure to address the spatial origin of modulus reduction.

Here, we report spatially resolved measurements of radial elastic modulus in MWNTs exhibiting uniform (AD-grown) and highly nonuniform (CVD-grown) radial microstructures using ultrasonic force microscopy (UFM). CVD-grown MWNTs exhibited local variations in the radial elastic modulus that were statistically correlated with diameter variation and were an order of magnitude larger than radial elastic modulus variations in comparable AD-grown MWNTs. Specifically, radial elastic modulus variations in CVD-grown MWNTS were inversely correlated with local increases in nanotube diameter, exhibiting an average normalized cross-correlation of -0.68 ± 0.05 compared to a value of 0.05 ± 0.18 for AD-grown MWNTs. These measurements indicate that modulus reduction in MWNTS exhibiting nonuniform radial microstructures results specifically from increased defect density associated with positive radial gradients. The average radial elastic moduli measured from both types of MWNTs studied were in reasonable agreement with prior work.

CVD-grown MWNTs were grown on SiO_2 substrates with a deposition technique reported earlier[10] and were dissolved, purified, and redispersed on clean, oxidized (100) Si wafer samples for imaging.[11] MWNTs were also grown via conventional AD synthesis, and the sample was purified and dispersed on clean oxidized (100) Si wafers. Outer MWNT diameters measured via AFM ranged from 20 to 50 nm. Transmission electron microscopy (TEM) imaging of similar

* Corresponding author. E-mail: rgeer@uamail.albany.edu.
[†] University at Albany.
[‡] Rensselaer Nanotechnology Center, Rensselaer Polytechnic Institute.
[§] Department of Materials Science and Engineering, Rensselaer Polytechnic Institute.
[||] Current address: Northwestern University Institute of Nanotechnology, Evanston, IL 60208.

10.1021/nl072002o CCC: $37.00
Published on Web 11/20/2007

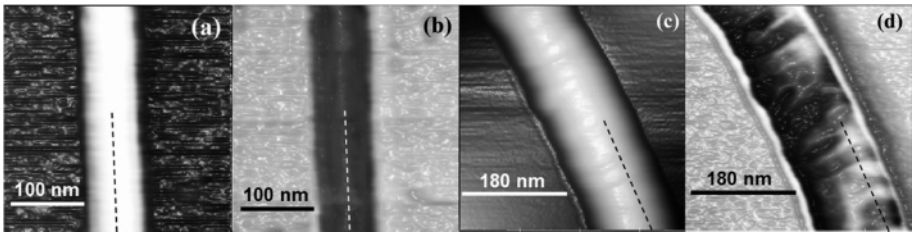

Figure 1. (a) AFM topography scan of an AD MWNT on a SiO_2-coated Si wafer. (b) UFM image of an AD MWNT acquired simultaneously with topography scan shown in (a). (c) AFM topography scan of a CVD-grown MWNT on a similar substrate. (d) UFM image of a CVD-grown MWNT acquired simultaneously with topography scan shown in (c). The relative UFM image contrast on the MWNTs is dominated by radial elastic modulus variations. Note the strong variations of the UFM image contrast of the CVD MWNT compared to that of the AD MWNT.

CVD-grown MWNTs revealed ratios of the outer diameter to inner diameter of 2.0 ± 0.4.

Topographic AFM and UFM images of AD and CVD-grown MWNTs are shown in Figure 1. The average measured diameter of the AD MWNT (Figure 1a) is 22 nm and varies by $\pm$ 0.4 nm along its axis. The height (*z*-axis) resolution of the AFM is less than 0.1 nm. The CVD MWNT (Figure 1c) exhibits a 48 nm diameter and varies by $\pm$ 2.5 nm along its axis. The UFM scan of the AD MWNT (Figure 1b) exhibits a uniform contrast well below that of the SiO_2 substrate indicative of its reduced contact stiffness and surface adhesion. The UFM image of the CVD MWNT differs starkly, revealing a wide intratube variation of surface mechanical contrast. Axial "bands" of alternating image contrast are apparent in addition to regions of overall depressed UFM contrast. (The difference in UFM contrast uniformity between the AD-grown and CVD-grown tubes was observed over the entire range of applied tip forces and ultrasonic vibration amplitudes.) Frictional force imaging was simultaneously acquired (not shown) and revealed no significant contrast variation over the MWNTs, implying the origin of the contrast in Figure 1d results from local variations in radial modulus, not surface adhesion. As with previous applications of ultrasonic-based AFM, experimental care was taken here to differentiate mechanical contrast from topographic artifacts.[12,13] Local changes in the tip−surface contact area can modify UFM contrast when the tip radius of curvature approaches or exceeds that of the surface.[14] This effect results in the bright "halo" evident at the edges of the CVD-grown MWNT (Figure 1d) and, to a lesser extent, the AD-grown tube. The topography on the uppermost portions of all MWNTs studied exhibited surface radii of curvature substantially larger than that of the tip, eliminating topographic artifacts as a contributor to the UFM contrast. Similar UFM contrast features have been observed for CVD-grown nanotubes exhibiting radial nonuniformities.[11]

To quantify the mechanical contrast of Figure 1d differential UFM was used to extract local radial modulus by measuring the relative change in UFM threshold amplitude as a function of applied tip force.[15] Figure 2 plots the applied tip force versus the variation of UFM threshold amplitude from a point of the CVD MWNT (solid triangles) and the SiO_2 substrate (solid circles). The AFM tip deflection measured during the UFM waveform ramp (Figure 2 inset) documents the force-dependent threshold amplitude. The

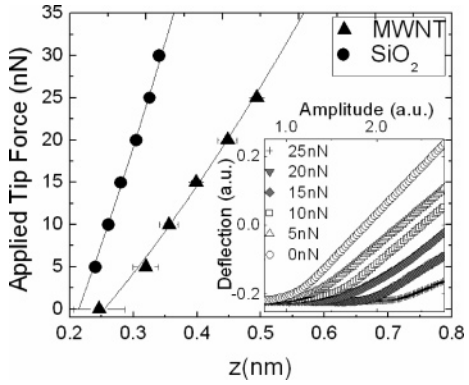

Figure 2. Variation of applied AFM tip force (nN) as a function of indentation (threshold variation) determined for the CVD MWNT (filled triangles) and the SiO_2-coated Si substrate (filled circles). Inset: AFM tip deflection as a function of ultrasonic amplitude for increasing tip force illustrating the change of threshold amplitude with applied tip force.

error bars in the main plot result, primarily, from threshold amplitude variation.

The tip-force/threshold-amplitude data, measured in the dynamically damped mode, in Figure 2 represents a force-displacement curve similar to AFM-based nanoindentation. Quantitative calibration for d-UFM has been shown to be highly accurate[16,17] for cases where calibration standards are similar to the materials under investigation. However, due to the significant topographic and mechanical modulus variations between the tip-substrate (SiO_2) contact and the tip-MWNT contact a calibration approach is undesirable. Instead, the Hertzian model describing the deformation of two curved bodies in contact (see ref 18; also applied in refs 8 and 9) has been used to analyze the force-displacement data of Figure 2.

The solid lines in Figure 2 represent a best fit of the force-threshold amplitude curve based on the Hertzian model with the measured displacement, *z*, corresponding to the sum deformation of the tip and nanotube, δ. The analysis yields a value of 75 ± 18 GPa for the Young's modulus of the SiO_2 substrate and a value of 21 ± 7 GPa for the radial modulus of the CVD MWNT. Absolute calibration error of the laser vibrometer is the primary contribution to the uncertainty of both quantities. The MWNT radial moduli measured here agree well with literature within experimental error. Shen et al. reported MWNT radial moduli of 5−10 GPa although the indentation forces used there were an order

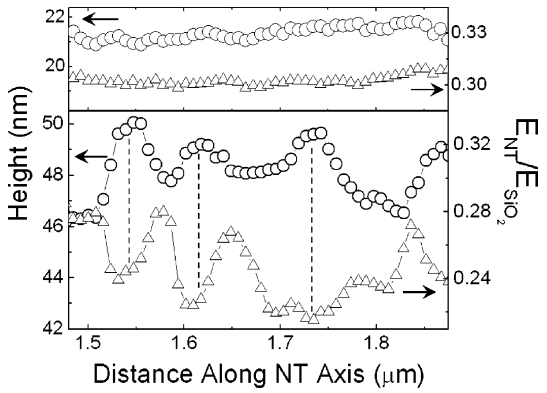

Figure 3. (Top) Topography profile (open circles) and relative radial modulus profile (open triangles for an AD-grown MWNT measured via AFM and UFM, respectively, along the dashed lines in Figure 1a,c. (Bottom) Topography profile (open circles) and relative radial modulus profile (open triangles for an AD-grown MWNT measured via AFM and UFM, respectively, along the dashed lines in Figure 1b,d. For the CVD MWNT, note the correlation between the local increase in nanotube diameter and the decrease in modulus. Vertical dashed lines are a guide to the eye.

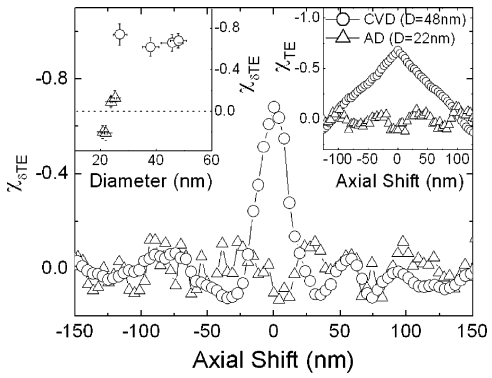

Figure 4. Normalized axial cross-correlation between the spatial derivatives of topographic and radial modulus maps from a CVD-grown MWNT (open circles) and an AD-grown MWNT (open triangles). No correlation between topographic variation and radial modulus variation is evident in the AD-grown MWNT while substantial negative correlation exists for the CVD-grown MWNT. Upper right inset: normalized axial cross-correlation between the topographic and radial modulus maps from a CVD-grown MWNT in agreement with the cross-correlation of the corresponding spatial derivatives. Upper left inset: normalized cross-correlation of the topographic and radial modulus variation as a function of MWNT diameter for CVD-grown tubes (open circles) and AD-grown tubes (open triangles).

of magnitude larger than this work and complicate a direct comparison.[8] Palaci et al. reported asymptotic radial modulus for MWNTS of 30 ± 10 GPa.[9] Yu et al. likewise measured radial moduli of an MWNT but obtained relatively low values (0.3−4 GPa) that were possibly attributable to low wall thickness.[7]

The force-displacement analysis for the data in Figure 2 yielded values for the tip/SiO_2 and tip/MWNT adhesion forces of 35 ± 7 and 15 ± 4 nN, respectively. The former value agrees well with direct tip/SiO_2 adhesive force measurements recently reported by Huebner et al. when normalized for tip/surface contact area,[19] supporting the validity of the Hertzian model, while the latter value is in reasonable agreement with ref 9.

Utilizing the aforementioned analysis, axial profiles of the radial modulus were obtained for CVD and AD MWNTs (along the dashed lines in AFM/UFM panels of Figure 1) and are shown in Figure 3 with corresponding height profiles.[16] Along these profile sections, the average heights of the AD and CVD MWNTS were 21.4 ± 0.3 and 47.9 ± 2.4 nm, respectively. Likewise, the average radial modulus (relative to SiO_2) was 0.30 ± 0.06 (AD) and 0.25 ± 0.08 (CVD). The majority of the absolute error is associated with ultrasonic amplitude calibration. Relative errors were an order of magnitude smaller. The radial elastic modulus of the CVD-grown MNWT modulus profile in Figure 3 ranged from 16 to 23 GPa. In contrast, the radial elastic modulus of the AD-grown MWNT changed by approximately 0.7 GPa across the profile (only slightly larger than the relative error of the radial modulus measurement) and represents an order-of-magnitude reduction.

A striking feature of Figure 3 is the inverse correspondence between local changes in CVD-grown MWNT radial modulus and MWNT diameter. To evaluate the statistical validity of this observation, a normalized cross-correlation function analysis was carried out between the topographic and radial modulus variations from four AD-grown MWNTs and four CVD-grown MWNTs. For each tube, 500 × 500 nm^2 areas of simultaneously acquired topographic and radial modulus images and corresponding spatial derivative maps were analyzed for cross-correlation defined as[20]

$$\chi(x,y) = \frac{\sum_{k,l} (I_a(k,l) - \bar{I}_a)(I_b(k+x, l+y) - \bar{I}_b)}{[(\sum_{k,l} (I_a(k,l) - \bar{I}_a)^2)(\sum_{k,l} (I_b(k+x, l+y) - \bar{I}_b)^2)]^{1/2}}$$

where $I_a(k,l)$ and $I_b(k + x, l + y)$ represent two spatial pixel maps shifted by (x, y) and $\bar{I}_a$ and $\bar{I}_b$ are the corresponding image pixel averages. A direct computation approach was utilized to evaluate $\chi(x,y)$ between 150 × 150 nm^2 offset image sections within the original 500 × 500 nm^2 scans to avoid spurious effects of Fourier transforms.[21]

The normalized cross-correlation function varies between 1 and −1 representing complete direct or inverse image correlation, respectively. The position of the maximum in χ corresponds to the relative spatial shift of the correlated components of the two image sections.[22] In Figure 4, the average cross-correlation of the spatial derivatives of the MWNT diameter and radial modulus ($\chi_{\delta TE}$) is plotted as a function of relative shift along the long axis of the nanotube for the CVD and AD MWNTs shown in Figure 1. No substantial correlation is observed for the AD MWNT (open triangles). In contrast, a clear correlation ($\chi_{\delta TE}(0)$) = −0.68 ± 0.07) is exhibited for the CVD MWNT. The position of the peak at a zero axial shift is important, signifying a direct correlation between topography and radial modulus. The algebraic sign confirms the trend observed in Figure 3: local increases in MWNT diameter lead to a reduction in local

modulus. The upper right inset in Figure 4 displays the cross-correlation function between the calibrated topography and radial modulus scans (χ_{TE}) and agrees with the spatial derivative cross-correlation. The peak in χ_{TE} likewise occurs at zero axial shift. The broadening of this peak results from the relatively small percentage change in diameter compared to that of the radial modulus over the image. The upper left inset of Figure 4 plots $\chi_{\delta TE}(0)$ as a function of diameter for four AD MWNTs (open triangles) and four CVD MWNTs (open circles). The correlation between diameter variation and radial modulus variation is consistent among both sets of MWNTs confirming and validating the trend observed in Figure 3.

It is well established that the additional curvature introduced in the C−C sp^3 bonds of carbon MWNTs and SWNTs is manifested by an increase in radial modulus. Although this is contrary to the data in Figures 3 and 4, curvature-induced variations in radial MWNT moduli are only expected for nanotubes with radii less than 3−4 nm, well below what is considered here, and can be ruled out as a cause for the observed relationship between local MWNT radial modulus and diameter. Rather, this is driven by other mechanisms. One possible reason is local variation in wall thickness. This cannot be directly confirmed because simultaneous UFM mapping and TEM imaging is not possible with our approach owing to the need for a mechanically rigid and inertially robust substrate.[23] However, there is no experimental evidence from the MWNTs studied here that the overall wall thickness varies inversely with nanotube diameter. Even if such were the case, recent results from Hertel and co-workers[24] suggests that radial modulus is independent of diameter (for a wide range of wall thicknesses) and roughly equivalent to that of *c*-axis graphite.[9]

A more likely explanation for the observed radial modulus behavior is the relative concentration of point and line defects. Gao et al. attributed the bending-modulus reduction for CVD MWNTs exhibiting an irregular radial microstructure (termed bamboo by those authors) to increased defect density, not wall thickness variation.[6] An increased defect density with local irregularities in MWNT diameter is also consistent with recently reported TEM analyses of CVD-grown MWNTs for which significant crystalline defects (alignment discontinuities of the graphitic planes) were observed in regions of varying diameter.[25] Although qualitative, these comparisons support the experimental observation that local defect concentrations associated with increased MWNT diameter is the primary source for the observed radial modulus reduction.

In conclusion, we report spatially resolved measurements of radial elastic modulus in MWNTs exhibiting smooth (grown by AD) and highly nonuniform radial microstucture (grown by CVD). CVD MWNTs exhibit strong variations in the radial elastic modulus, which are inversely correlated to local changes in tube diameter, indicating that the elastic modulus reduction previously observed for MWNTs exhibiting nonuniform microstructure originates from increased defect density associated with positive radial gradients. This is supported, indirectly, by TEM imaging of similar MWNTs.

Acknowledgment. This work was supported by the Nanoscale Science and Engineering Initiative of the National Science Foundation under NSF Awards DMR-0117792, DMR-0642573, DMR-0320569, and DMR-0303764, by the Semiconductor Research Corporation Focus Center Research Program, and the New York State Office of Science, Technology, and Academic Research.

Supporting Information Available: The details of the UFM experimental configuration and data acquisition protocol as well as the details of the Hertzian model used to analyze the differential UFM force-response data are included in online documentation. This material is available free of charge via the Internet at http://pubs.acs.org.

References

(1) Iijima, S. *Nature* **1991**, *354*, 56.
(2) Treacy, M. M.; Ebbesen, T. W.; Gibson, J. M. *Nature* **1996**, *381*, 678.
(3) Yao, N.; Lordi, V. *J. Appl. Phys.* **1998**, *84*, 1939.
(4) Wong, E. W.; Sheehan, P. E.; Lieber, C. M. *Science* **1997**, *277*, 1971.
(5) Akita, S.; Nishijima, H.; Kishida, T.; Nakayama, Y. *Jpn. J. Appl. Phys.* **2000**, *39*, 3724.
(6) Gao, R.; Wang, Z. L.; Bai, Z.; de Heer, W. A.; Dai, L.; Gao, M. *Phys. Rev. Lett.* **2000**, *85*, 622.
(7) Yu, M.; Kowalewski, T.; Ruoff, R. S. *Phys. Rev. Lett.* **2000**, *85*, 1456.
(8) Shen, W.; Jiang, B.; Han, B.; Xie, S. *Phys. Rev. Lett.* **2000**, *84*, 3634.
(9) Palaci, I.; Federigo, S.; Brune, H.; Klinke, C.; Chen, M.; Riedo, E. *Phys. Rev. Lett.* **2005**, *94*, 175502.
(10) Wei, B. Q.; Vajtai, R.; Jung, Y.; Ward, J.; Zhang, R.; Ramanath, G.; Ajayan, P. M. *Chem. Mater.* **2003**, *15*, 1598.
(11) Muthuswami, L.; Ajayan, P. M.; Geer, R. E. *Mater. Res. Soc. Symp. Proc.* **2003**, *778*, U5.10.
(12) Burnham, N. A.; Kulik, A. J.; Gremaud, G.; Gallo, P.-J.; Oulevey, F. *J. Vac. Sci. Technol., B* **1996**, *14*, 794.
(13) Rabe, U.; Amelio, S.; Kester, E.; Schere, V.; Hirsekorn, S.; Arnold, W. *Ultrasonic* **2000**, *38*, 430.
(14) Kolosov, O. V.; Castell, M. R.; Marsh, C. D.; Briggs, G. A. D.; Kamins, T. I.; Williams, R. S. *Phys. Rev. Lett.* **1998**, *81*, 1046.
(15) Dinelli, F.; Biswas, S. K.; Briggs, G. A. D.; Kolosov, O. V. *Phys. Rev. B* **2000**, *61*, 13995.
(16) Muthuswami, L.; Geer, R. E. *Appl. Phys. Lett.* **2004**, *84*, 5082.
(17) Zheng, Y.; Geer, R. E.; Dovidenko, K.; Kopycinska-Müller, M.; Hurley, D. C. *J. Appl. Phys.* **2006**, *100*, 124308.
(18) Boresi, A. P.; Sidebottom, O. M. *Advanced Mechanics of Materials*; John Wiley & Sons: New York, 1984; p 609.
(19) Hübner, R.; Eichenlaub, S.; Rastegar, A.; Geer, R. E. *Proc. SPIE Int. Soc. Opt. Eng.* **2006**, *6349*, 63493E.
(20) Gonzalez, R. C.; Woods, R. E. *Digital Image Processing*, 3rd ed.; Addison-Wesley: Reading, MA, 1992; p 585.
(21) Mantooth, B. A.; Donhauser, Z. J.; Kelly, K. F.; Weiss, P. S. *Rev. Sci. Inst.* **2002**, *73*, 313−37.
(22) Barnea, D. I.; Silverman, H. F. *IEEE Trans. Comput.* **1972**, *21*, 179−186.
(23) Ultra-thin supporting membranes suitable for TEM (carbon, Si_3N_4, Si, etc.) introduce problematic mechanical resonances for local ultrasonic imaging and greatly complicate combined TEM/UFM of MWNTs. Alternative approaches to resolve this challenge are currently being undertaken by the authors.
(24) Hertel, T.; Walkup, R. E.; Avouris, P. *Phys. Rev. B* **1998**, *58*, 13870.
(25) Ludovico, M.; Dell'Acqua-Bellavitis, J.; Ballard, D.; Vajtai, R.; Pulickel, M.; Ajayan, R. W. Siegel *J. Phys. Chem. C* **2007**, *111*, 2623−2630.

NL072002O